Astronomy & Astrophysics

Analysis of the TiO isotopologues in stellar optical spectra

Ya. V. Pavlenko[1,2], Sergei N. Yurchenko[3], Laura K. McKemmish[4], and Jonathan Tennyson[3]

[1] Main Astronomical Observatory of NAS Ukraine, 27 Zabolotnoho, Kyiv 01137, Ukraine
  e-mail: yp@mao.kiev.ua
[2] Centre for Astrophysics Research, University of Hertfordshire, College Lane, Hatfield, AL10 9AB, UK
[3] Department of Physics and Astronomy, University College London, London WC1E 6BT, UK
[4] School of Chemistry, University of New South Wales, 2052 Sydney, Australia

ABSTRACT

Context. We used the new ExoMol TiO rovibronic line lists to identify and model TiO isotopologue features in spectra of M dwarfs.
Aims. We investigate problems involving the computation of electronic bands for different isotopologues of TiO by modelling optical spectra of late-type stars. Based on this, we determine their Ti isotopic abundances and compare the TiO isotopologue spectra computed using line lists by different authors.
Methods. We fitted theoretical synthetic spectra to the observed stellar molecular bands of TiO. We modelled spectra of two M dwarfs, GJ 15A (M1V) and GJ 15B (M3 V), to determine Ti isotopic ratios in their atmospheres.
Results. We demonstrate the accuracy of the ExoMol TOTO line list for different isotopologues of TiO and the possibility of determining accurate Ti isotope abundances in a number of spectral ranges. The 7580–7594 Å spectral range seems particularly useful, with two atomic lines of Fe I and molecular band heads of ^{50}Ti O, ^{49}Ti O, ^{48}Ti O, and ^{47}Ti O clearly observable in our two M-dwarf spectra. We determine non-solar Ti isotopic ratios of ^{46}Ti, ^{47}Ti, ^{48}Ti, ^{49}Ti, and ^{50}Ti of 7.9, 5.2, 72.8, 7.9, and 6.2 for GJ 15A and 7.4, 4.2, 76.6, 5.8, and 6.0 for GJ 15B with an accuracy of ±0.2. [Ti] = 0.040 and 0.199 and within an accuracy of ±0.10 were also determined for GJ 15A and GJ 15B, respectively.
Conclusions. We find that the ExoMol TOTO TiO line list (a) describes the fine details in line position and intensity of the M-dwarf spectra better than other available TiO line lists, (b) correctly reproduces the positions and intensities of the TiO isotopologue band heads observed in M-dwarf spectra, and (c) can be used to determine Ti isotope abundances in atmospheres of M stars.

Key words. astrochemistry – stars: late-type – stars: abundances – molecular data – nuclear reactions, nucleosynthesis, abundances

1. Introduction

Naturally occurring titanium, the element of nuclear charge 22, is composed of five stable isotopes, ^{46}Ti, ^{47}Ti, ^{48}Ti, ^{49}Ti and ^{50}Ti. Thus far, nuclide abundances of these elements in the Solar System formed 4.56 Ga ago have been measured with high accuracy. ^{48}Ti is the most abundant isotope (73.72% natural abundance) with Solar System isotopic ratios of ^{46}Ti, ^{47}Ti, ^{48}Ti, ^{49}Ti and ^{50}Ti of 8.249, 7.372, 73.72, 5.409, and 5.185 (Lodders et al. 2009). Similar numbers are given by De Bievre & Taylor (1993). Atoms of Ti isotopes in the low-temperature regime ($T < 4000$ K) are bound in TiO molecules, and molecular bands of TiO are used to assess the low-mass stars and brown dwarfs of spectral class M. Twenty-one radioisotopes of Ti have also been characterised, and the most stable is ^{44}Ti with a half-life of 60 yr. ^{44}Ti is observed in the supernova (SN) remnants, see Mochizuki et al. (1999). This isotope offers one of the most direct probes into nucleosynthesis environments in the interior of exploding stars, when the associated gamma-ray activities in the explosion remnant are detected and translated back into the isotopic abundances at the time of the explosion (Mochizuki & Kumagai 2004; Mochizuki et al. 1999).

Details of the galaxy nucleosynthesis of Ti isotopes are described in many papers, see Hughes et al. (2008), for example. Sources of the stable Ti isotopes are known well, see Table 1 in Alexander & Nittler (1999) and Woosley & Weaver (1994):
– ^{46}Ti and ^{47}Ti are formed during explosive oxygen and silicon burning, respectively, in SN types II and Ia;
– ^{48}Ti is formed by explosive Si burning in type II SN;
– ^{49}Ti is formed by the explosive Si burning in type II SN;
– ^{50}Ti is formed in nuclear burning in type Ia SN.

Mochizuki et al. (1999) noted that long-lived isotopes with mean lifetimes of about 10^6 yr or longer will reflect a superposition of different SNe at different times, mixed with interstellar matter. Consequently, abundances in an individual object are formed by different branches of many processes at long timescales. Only short-lived isotopes will clearly trace individual events.

The classical model of Timmes et al. (1995) suggested that most stable Ti isotopes were under-produced with respect to solar values: relative to ^{48}Ti and the Solar System isotopic ratios, the predicted abundances of ^{46}Ti are a factor of two to high, those of ^{47}Ti are a factor of three too low, those of ^{49}Ti are an exact match, and those of ^{50}Ti are a factor of 2 too low. Isotopic ratios were predicted to decline with decreasing [Fe/H] by a factor of 8 for ^{46}Ti, a factor of 6 for ^{47}Ti, a factor of 2 for ^{49}Ti, and a factor of 30 for ^{50}Ti between [Fe/H] = 0 and −1. The degree of this underproduction depends on many theoretical assumptions, see Hughes et al. (2008).

Essentially, modelling the abundances of TiO isotopologues (Lambert et al. 1972; Wyckoff & Wehinger 1972; Lambert & Luck 1977; Clegg et al. 1979; Valenti et al. 1998) is the only way to extract Ti isotopic abundances from M stars. It is a very hard task to determine Ti isotopic ratios from the analysis of atomic lines because different isotopic lines have small isotopic

Table 1. Parameters of stars taken from the literature.

$T_{\rm eff}$	log g	[Fe/H]	CompStar	Reference
			GJ 15A	
3606	4.93	−0.27		Passegger et al. (2018)
3669		−0.29	SUN	Gaidos et al. (2014)
3693		−0.26	SUN	Gaidos & Mann (2014)
3551		−0.28		Terrien et al. (2015)
3760		−0.23		Terrien et al. (2015)
3368		−0.26		Terrien et al. (2015)
3603		−0.30	SUN	Mann et al. (2015)
3988				Gaia Collaboration (2018)
			GJ 15B	
3283	5.11	−0.19		Passegger et al. (2018)
3282		−0.17	SUN	Gaidos et al. (2014)
3540	5.30	−0.20	SUN	Zboril & Byrne (1998)
3254		−0.20	SUN	Gaidos & Mann (2014)
3218		−0.30	SUN	Mann et al. (2015)
		−0.08	SUN	Newton et al. (2014)
3679	4.92	−1.15	SUN	Prugniel et al. (2011)
3630	4.71	−0.88	SUN	Koleva & Vazdekis (2012)
3330	5.08	−1.40	SUN	Cenarro et al. (2007)
3636				Gaia Collaboration (2018)

shifts, see Kobayashi et al. (2019) and references therein. The broadening of spectral lines by macroturbulence in the stellar atmospheres as well as any notable rotation of stars almost prevents us from separating the atomic spectra of different isotopes (Tennyson 2019).

Accurate molecular line lists, that is, lists of energy levels and the intensity of spectral transitions, are crucial for correctly modelling a variety of astrophysical phenomena, including stellar photospheres and the atmospheres of extra-solar planets. Transition metal diatomic line lists are particularly difficult because of the large number of coupled low-lying electronic states (Tennyson et al. 2016b). TiO line lists are particularly important for studies of M-dwarfs (Pavlenko et al. 1995; Allard et al. 2000), and a number of them have been constructed (Schwenke 1998; Plez 1998; Ryabchikova & Pakhomov 2015; McKemmish et al. 2019). The most recent of these is the TOTO line list of McKemmish et al. (2019), which was computed as part of the ExoMol project (Tennyson & Yurchenko 2012).

TiO line lists were first used to extract the titanium abundance in the 1970s, for instance, by Lambert et al. (1972), Wyckoff & Wehinger (1972), Lambert & Luck (1977) and Clegg et al. (1979). These studies were limited by the quality of the underlying line list, however, leading Valenti et al. (1998) to introduce isotope-dependent shifts to the line positions. These modifications should no longer be necessary with modern line list development techniques.

The majority of previous studies used the spectral range 7053.5–7055 Å to quantify the abundance of TiO isotopologues and thus the Ti abundance. However, the quality and availability of new and more accurate TiO molecular spectroscopic data and analysis techniques means that the suitability of this spectral region should be reconsidered.

We note that detailed comparisons with high-resolution M-dwarf spectra performed by McKemmish et al. (2019) showed that their TOTO line list performed much better than the earlier line lists, particularly in matching line positions. These

comparisons concentrated on the main isotopologue ^{48}Ti. We assess here the utility of the TOTO line list for modelling TiO isotopologue spectra in M dwarfs. A more detailed discussion of the TOTO line list is given below. We also extended the comparison of the quality of TiO isotopologue line lists computed by different authors, see Sect. 2.1, by comparing fits of computed spectra to the observed spectra.

The nearest and brightest stars are among the best studied and hold a special place in popular imagination. The discovery of planets orbiting these stars tells us that the solar neighborhood is potentially rich with exoplanet systems; see Howard et al. (2014) for the complete list of known exoplanet-hosting stars within 7 pc. The great advantage of investigating these stars is that it is possible to undertake extensive campaigns to characterise them using a combination of high-resolution optical spectroscopy, near-infrared (NIR) spectroscopy, long-baseline optical/infrared interferometry, and high-cadence, broadband optical photometry. Even for the history of our own planetary system, the Ti isotopic studies are of great importance. Zhang et al. (2012) found that the ratio of ^{50}Ti to ^{47}Ti of the Moon is identical to that of the Earth within about four parts per million, which is only 1/150 of the isotopic range documented in meteorites; see Table 2 in Zhang et al. (2012). This means that the Moon-forming giant impactor, that is, hypothetical Theria, would be of the same isotopic composition as our Earth. Theory predicts that the Moon is constructed mostly (40–75%) of the impactor materials. However, the observed identical titanium (and oxygen) isotopic compositions on Earth and the Moon are surprising in light of what we think we know about planet formation and formation of the Moon after a giant impact; see Taylor (2012). We expect growing interest of exoplanetary astrophysicists in isotopic studies of Ti and other elements.

We study the TiO isotopologues in spectra of the wide binary system GJ 15 A,B. GJ 15A (also known as Groombridge 34A, V* GX And, HD 1326A, HIP 1475, BD+43 44A, and *Gaia* DR2 385334230892516480) is a cool red dwarf of type M1. The other member of this binary star system, GJ 15B (also known as Groombridge 34B, V* GQ And, HD 1326B, BD+43 44B, and *Gaia* DR2 385334196532776576) is fainter and has a spectral type of M3.5 V (Reid et al. 1995). Lippincott (1972) measured a small astrometric segment of their orbit, giving an AB separation of 146 AU and an orbital period of 2600 yr. Based on an imaging search for companions at 10 μm with MERLIN at Palomar, van Buren et al. (1998) ruled out additional companions to A with projected separations of 9–36 AU with $T_{\rm eff} > 1800$ K ($M > 0.084\ M_\odot$). Gautier et al. (2007) found no IR excess for GJ 15A at 24, 70, or 160 μm. Because GJ 15A is a bright nearby star, many teams have provided studies of this component of the binary system; these are summarized in Table 1.

2. Procedure

We model optical spectra of M dwarfs. TiO features dominates here, but other molecules also provide notable features in different spectral ranges, see Pavlenko (2014)[1]. In addition to TiO, absorption by molecular bands of VO, CaH, CrH, MgH, and other hydrides from the Kurucz database (Kurucz 2011) were accounted for in our computations, as well as absorption by atomic lines taken from the VALD (Ryabchikova & Pakhomov 2015).

---

[1] Colour plots are available at `www.mao.kiev.ua/staff/yp/Results/M-stars/mb.htm`

2.1. Titanium oxide line lists

In the following, we analyse different line lists for monosubstituted isotopologues of TiO computed using the Toto line lists of McKemmish et al. (2019). The Toto line lists were constructed for the main isotopologues of titanium oxide (TiO), namely ^{46}TiO, ^{47}TiO, ^{48}Ti O, ^{49}TiO, and ^{50}TiO. Here and below we assume that oxygen is represented by its ^{16}O isotope as other oxygen isotopes are much less abundant in both the solar vicinity (De Bievre & Taylor 1993; Lodders et al. 2009) and the majority of the known astrophysical objects.

The Toto line lists contain transitions with wavenumbers up to 30 000 cm^{-1}, that is, longwards of 330 nm, and include all dipole-allowed transitions between 13 low-lying electronic states (X $^3\Delta$, a $^1\Delta$, d $^1\Sigma^+$, E $^3\Pi$, A $^3\Phi$, B $^3\Pi$, C $^3\Delta$, b $^1\Pi$, c $^1\Phi$, f $^1\Delta$, and e $^1\Sigma^+$). The Toto rovibronic line positrons were constructed using potential energy curves as simple Morse oscillators with constant diagonal and off-diagonal spin-orbit and other coupling terms fitted to match known empirical energy levels and ab initio curves where experimental data were unavailable. Accurate line intensities were generated using ab initio dipole moment curves. Final line lists were computed using the variational nuclear-motion program Duo (Yurchenko et al. 2016), where various couplings were explicitly included. The Toto line lists are appropriate for temperatures below 5000 K and contain about 60 million transitions for the main TiO isotopologue; higher temperature data are not required as TiO bands disappear in stellar spectra above about 4200 K due to dissociation of the titanium oxide molecule.

The variational procedure described above is known not to provide sufficiently accurate TiO spectra for high-resolution studies, see Hoeijmakers et al. (2015), for example. Therefore, McKemmish et al. (2019) used empirical energy levels they had obtained previously (McKemmish et al. 2017) using the so-called measured active rotation-vibration energy levels (MARVEL) procedure (Furtenbacher et al. 2007; Tóbiás et al. 2018) to improve the Toto energy levels and thus the predicted transition frequencies. MARVEL energies are only available for ^{48}Ti^{16}O; the comparisons made by McKemmish et al. (2019) show that these corrected frequencies reproduce the majority of stellar features associated with TiO very well.

For the other isotopologues, McKemmish et al. (2019) adopted the method of Polyansky et al. (2017) and shifted the isotopologue energy levels by the observed (MARVEL) minus calculated value obtained for ^{48}Ti O. They made no allowance for any shifts associated with breakdown of the Born-Oppenheimer approximation. McKemmish et al. (2019) provided initial evidence for the success of this approach in the region 14 145–14 175 cm^{-1} by comparing experimental TiO spectra to cross sections generated using the Toto line list and demonstrated that the weak peaks in the experimental spectra are isotopologue peaks. Our study provides a stringent test of how well this method works in practice.

The Toto TiO spectroscopic data is given in two datasets, a states and a transitions file (Tennyson et al. 2016a). The huge amount of data is not easy to use directly in astrophysical computations. Therefore we converted the Toto line data into the format of our synthetic spectra computation programs, see Table A.1. Furthermore, to reduce the number of lines that might effectively absorb radiation in the lower temperature regime we considered here, we selected only stronger lines using the cutoff parameter $\alpha > 10-6$, here

$$\alpha = gf * \exp(-E''/kT), \tag{1}$$

where f is the oscillator strength of line in absorption, g is the statistical weight of the lower level, and E'' is the lower state energy, $T = 3000$ K. After we computed the wavelength of the lines in vacuum, they were shifted to the air wavelength scale using the formulae of Ciddor (1996). In the following we use the air wavelength scale.

To estimate the quality of the different line lists, we compared fits to the observed spectra of GJ 15A and GJ 15B using line lists of TiO isotopologues computed by Schwenke (1998), labelled S98 below, Plez (1998), an updated version was taken from the web page[2], labelled P12 below, and McKemmish et al. (2019), the Toto line list. The results of our comparison of synthetic spectra computed with different lists with observed spectra are given in Sects. 3.2.1 and 3.2.2.

2.2. Observed spectra

For the analysis, we used high-resolution spectra of both stars from the CARMENES spectral library of Reiners et al. (2018). The CARMENES spectra cover the wavelength range 520–1710 nm at a resolution of at least $R = 80\,000$ or better. The spectra of GJ 15A and GJ 15B used in this work were observed with exposures in 61 and 198 s to obtain the comparable signal-to-noise ratio (S/N) of 68 and 54, respectively. We refer to Reiners et al. (2018) for more details. All theoretical spectra were shifted to account for the radial velocity of the appropriate star.

2.3. Synthetic spectra and model atmospheres

To generate synthetic spectra, we used the BT-Settl model atmosphere (Allard 2014). The procedure for computing synthetic spectra is described elsewhere; see Pavlenko (1997). We adopted the solar abundances of Anders & Grevesse (1989). Line profiles were computed using Voigt profiles, and damping constants were taken from the line list databases or computed in the framework of the Unsöld approximation. Synthetic spectra were computed in wavelength steps of 0.025 Å, where we adopted the micro-turbulent velocity of $V_t = 1$ km s^{-1}. Some numerical experiments showed a rather marginal dependence of our results on V_t. Our fitting procedure did not reveal any notable rotational velocities $v \sin i$, therefore the theoretical spectra were convolved with a pure Gaussian profile in order to model the instrumental broadening, see the next subsection. We fixed $T_{eff} = 3800$ K and $T_{eff} = 3500$ K for the A and B components, respectively. These values are not far from the *Gaia* 3869 and 3636 K (Gaia Collaboration 2018), respectively.

2.4. Fits to the observed spectra

The best fit to the observed spectra was achieved by the χ^2 procedure described elsewhere (Pavlenko 2014). We give a few details here to aid understanding of our procedure. As part of the fit, the function

$$S = \sum_{i=1}^{N} s_i^2 \tag{2}$$

is minimised, where $s_i = |F_i^{obs} - F_i^{comp}|$; F_i^{obs} and F_i^{comp} are the observed and computed fluxes, respectively, and N is the number of the wavelengths points used in the minimisation procedure. Three parameters were used in our minimisation procedure: the

---

[2] https://nextcloud.lupm.in2p3.fr/s/r8pXijD39YLzw5T?path=%2FTiOVALD

Table 2. Spectral ranges of our interest.

Sp. range	Wavelengths (Å), air	Wavenumber (cm^{-1})	El. system	(v'', v')
x_1	7053.5–7055	14 173.2–14 170.2	γ (A $^3\Phi$ – X $^3\Delta$)	(0,0)
x_2	7580–7594	13 188.8–13 164.5	γ (A $^3\Phi$ – X $^3\Delta$)	(0,1)
x_3	8194–8204	12 200.5–12 185.6	δ (b $^1\Pi$ – a $^1\Delta$)	(1,0)
x_4	8858–8862	11 286.0–11 280.9	δ (b $^1\Pi$ – a $^1\Delta$)	(0,0)
x_5	9720–9737	10 285.1–10 267.1	δ (b $^1\Pi$ – a $^1\Delta$)	(0,1)

Doppler shift measured in km s^{-1}, the flux scale normalisation parameter, and the full width at half maximum (FWHM) used for the smoothing Gaussian. They were determined for every fitted spectral range. In our analysis we omitted some spectral ranges that contained artifacts provided by strong noise, telluric absorption, bad pixels, etc. The minimisation sum S was computed on a 3D grid of radial velocity sets, flux normalisation factors, and FWHM parameters. Errors in the fit were evaluated as $\Delta S = \sum s_i / N$.

3. Results

3.1. Search for the best spectral ranges

Spectral features associated with isotopologues are difficult to see because they are faint and close to each other. The flux ratio method shows the strongest TiO absorption regions that should be analysed for the largest splitting. This should be complemented by observations of highest spectral resolution (>100 000) and highest S/N, see Valenti et al. (1998). It it worth noting here that usually, the macroturbulence in the atmospheres of late-type stars reduces the effective resolution to 70 000 or less. Generally, the use of flux ratios could provide an alternative approach, but restricting ranges to the band heads allows the procedure to focus on measuring isotopic ratios. It is possible that the use of much wider spectral ranges may offer reasonable statistics on the accuracy of the individual wavelengths in the new line list with its better quality.

On the other hand, going to the shorter wavelengths may also enhance the chances of finding high-quality high-resolution spectra in observational archives (HIRES, HARPS, etc.), see Valenti et al. (1998) and others referenced in the introduction. However, this approach requires very high accuracy of the input line lists and even minimum blending with other molecular lines, even from the same molecule, is likely to cause problems. In practice, the TiO optical spectrum comprises absorption bands of different systems, and the responses of these band systems to changes in the temperature structure of the model atmosphere are different because of the different excitations of the lower level of each transition. Furthermore, using small spectral ranges is better than using a cross-correlation across a wide spectral range, and the TiO line list is less accurate at shorter wavelengths than longer wavelengths because we lack reliable spectroscopic data for the molecular levels with high excitation, see McKemmish et al. (2019) Conversely, we know from experience that an analysis of the well-characterised isotopologue band heads across comparatively short spectral ranges allows increasing the accuracy of the abundance determination by modelling infrared molecular bands of CO and SiO, see Pavlenko et al. (2020) and references therein.

As a first step in our analysis, we therefore determined the spectral regions that are useful for an isotopic abundance

determination of Ti. To this end, we computed two spectra of fluxes: the first spectrum, F_{48}, contains absorption of ^{48}TiO only, while the second spectrum F_{all} contains all TiO isotopologues assuming the solar Ti isotopic ratios. Both spectra were smoothed by Gaussians with $R = 60000$ and are shown in Fig. 1 together with their flux ratios: $F_r = F_{all}/F_{48}$. The flux ratios across band heads should show the highest sensitivity to the isotopologue abundances. Here we consider several spectral ranges with $\lambda > 7000$ Å. At shorter wavelengths, spectra of M stars become more complicated due to interference between different molecular bands while their flux also drops noticeably bluewards. We denote the spectral ranges of interests as $x_1, x_2 \ldots x_5$ (see Table 2) and analyse the computed flux ratios in comparison with the observed X-shooter spectrum of GJ551 (Proxima Cen) as described by Pavlenko et al. (2017).

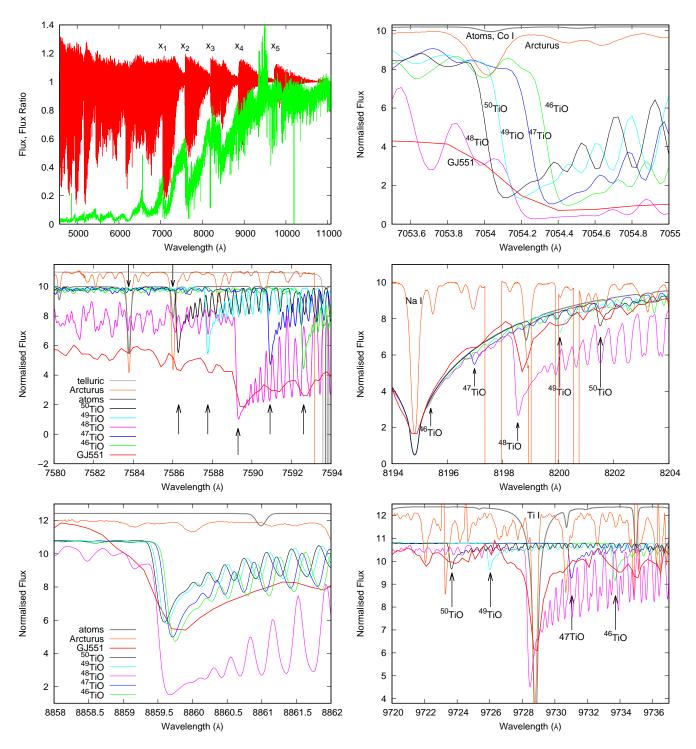### 3.1.1. Spectral range x_1: 7053.5–7055 Å

The main spectral feature of x_1 is formed by the TiO γ-system, that is, A $^3\Phi$ – X $^3\Delta$, (0,0) band with its leading red-degraded band head at 7054 Å. This spectral window was used for modelling sunspot spectra by Lambert et al. (1972), Omicron Ceti by Wyckoff & Wehinger (1972), Aldebaran by Lambert & Luck (1977), spectra of late-type dwarfs and giants by Clegg et al. (1979), studies of M dwarfs by Valenti et al. (1998), and spectra of local M dwarfs by Chavez & Lambert (2009). Unfortunately, the TiO band head in this region is formed by blends of unresolved components of TiO isotopologues, see the top right panel of Fig. 1, therefore we preferred to use wavelengths longer than the molecular head at 7054 Å. Furthermore, at the wavelength of the band head, there is a strong atomic line, clearly seen in the spectrum of Arcturus (Hinkle et al. 1995), which further complicates the analysis.

It is worth noting that this spectral range is also affected by absorption due to strong lines of the TiO γ' (0,1) band, which is a part of the B $^3\Pi$ – X $^3\Delta$ band system of the (0,0) band head at 6192.5 Å. A mixture of lines of the γ and γ' bands complicates the fine-structure analysis of the x_1 spectral range. Both bands are included in the ToTo line list.

3.1.2. Spectral range x_2: 7580–7594 Å

The head of the red-degraded (0,1) band of the γ-system (A $^3\Phi$ – X $^3\Delta$) is located at 7589 Å. Here we have some contribution from lines in the tail of the (0,0) TiO band, which becomes stronger at lower T_{eff}.

Generally speaking, the fluxes in the optical spectra of late-type dwarfs increase towards the red, therefore this spectral range is preferable. On the other hand, the strong telluric O$_2$ A-band absorption is located approximately at $\lambda = 7580$ Å (Rudolf et al. 2016). We note that the position of the molecular head in stellar

Fig. 1. *Top left*: observed X-shooter spectrum of GJ551 (green line) (Pavlenko et al. 2017) and flux ratio F_{48}/F_{all} (red line); the green line shows the observed X-shooter fluxes in the Proxima spectrum. $x_1, ...x_5$ mark our spectral ranges of interest. *Top right*: band heads of TiO isotopologues computed for a 2900/4.5/0.0 model atmosphere. All observed spectra are shifted to the zero radial velocity frame. *Middle panels*: theoretical spectra of bands of TiO isotopologues computed across the x_2 it (*right panel*) and x_3 (*left panel*) spectral ranges. Upward arrows show the positions of head bands of the TiO isotopologues. Downward arrows label two Fe I lines seen in absorption. *Bottom panels*: theoretical spectra of bands of TiO isotopologues computed across x_4 (*right panel*) and x_5 (*left panel*) spectral ranges. The positions of the molecular band heads are shown by arrows. In all panels the observed spectra of Acturus and Proxima Cen (GJ551) are shown by thin and thick red lines, respectively, to demonstrate the locations of notable atomic and molecular features in the observed spectra.

spectra reduced to the local coordinate frame varies depending on the relative radial velocity of the star. In the X-shooter spectrum of Proxima Cen obtained with long exposures, the O_2 molecular band is found at even shorter wavelengths, that is,

beyond 7580 Å. There are two atomic lines of Fe I in the x_2 spectral range that provide the means to determine accurate Doppler shifts that are important for the proper identification of the weak TiO isotopologue features.

As shown in the left middle panel of Fig. 1, features created by ^{50}TiO, ^{49}TiO, and ^{48}TiO are clearly seen in the computed HIRES spectra as well as in the X-shooter spectrum of intermediate resolution of Proxima. The heads of the isotopologue bands ^{46}TiO and ^{47}TiO can be seen only in the background of stronger lines belonging to the tail of ^{48}TiO in the HIRES spectra.

An additional advantage of the x_2 spectral region is the presence of two atomic Fe I lines at 7583.8 and 7586.0 Å, see the downward arrows in the middle left panel of Fig. 1. These lines are clearly seen in the Arcturus spectrum and can be used for an accurate wavelength reduction in cooler stars as well.

3.1.3. Spectral range x_3: 8194–8204 Å

The x_3 spectral range contains the (1,0) band head of the δ (b $^1\Pi$ – a $^1\Delta$) system of TiO. The main absorption feature here is formed by the reddest line of the subordinate Na I triplet at 8183.255, 8194.790, and 8194.823 Å (8200 Å triplet), see the right middle panel of Fig. 1. Interestingly, the molecular bands occur in reverse order in comparison to the γ band system; here the heads of the isotopologue bands occur in ascending order, from ^{47}TiO to ^{50}TiO.

Unfortunately, this structure of the x_3 spectral range complicates the detailed analysis of the weak molecular features created by the bands of TiO isotopologues. Subordinate Na I lines of the 8200 Å triplet are well-known indicators of the gravity in late-type dwarfs, but they depend on the effective temperature as well, see Schlieder et al. (2012). Likely, the x_3 wavelength range can be used for Ti isotopic analysis in spectra of lower gravity stars, in which Na I lines at 8200 Å should have weaker wings.

3.1.4. Spectral range x_4: 8858–8862 Å

The strong head of the (0,0) band of the δ system, that is, b $^1\Pi$ – a $^1\Delta$, is a notable observational feature in the x_4 range. Unfortunately, the wavelength shifts between heads of TiO isotopologue bands are small so that even in the HIRES spectra we can see only one band head formed by several TiO isotopologues bands. The tail of the composite molecular band provides some opportunities for detecting isotopologue lines that are notably shifted with respect to the ^{48}TiO lines; these can be seen in the 8881–8862 Å range where strong atomic or telluric lines are absent. On the other hand, these wavelengths are severely polluted by (0,0) FeH and CrH molecular lines of the FeH F $^4\Delta_i$ – X $^4\Delta_i$ and CrH A $^6\Sigma^+$ – X $^6\Sigma^+$ systems with band heads at 8694 and 8520 Å, respectively, see Pavlenko (2014).

3.1.5. Spectral range x_5: 9720–9737 Å

The x_5 spectral range contains the (0,1) band head of the δ (b $^1\Pi$ – a $^1\Delta$) system of TiO. The bottom right panel of Fig. 1 illustrates at least two problems of this wavelength range: (a) the spectrum is severely polluted by telluric absorption, and (b) the strong Ti I atomic line at 9728.32 Å seen in the spectrum of Arcturus and Proxima forms blend with a molecular band head of ^{48}TiO. On the other hand, the TiO isotopologue band heads are well spaced in wavelength. Again, molecular bands of higher mass isotopologues are shifted blue-ward, away from the strong ^{48}TiO band head. The x_5 spectral range can be used to determine ^{50}TiO and ^{49}Ti O abundances, but only in the of absence of telluric absorption at the wavelengths of their band heads. The ^{47}TiO and ^{46}Ti O band heads can be observed in the background of the stronger tail of the ^{48}TiO band. Again, the strong

telluric absorption makes it difficult to perform a fine-structure analysis of the weak molecular features across this spectral range.

3.2. Determination of Ti isotope abundances in the atmospheres of GJ 15A and GJ 15B

After selecting the best spectral ranges for the determination of Ti isotope abundances, we performed fits of our synthetic spectra to observed spectra of GJ 15A and GJ 15B in selected spectral ranges to demonstrate that they can be used to determine the abundances of Ti isotopes in their atmospheres. As before, we assumed that all oxygen atoms exist in the form ^{16}O.
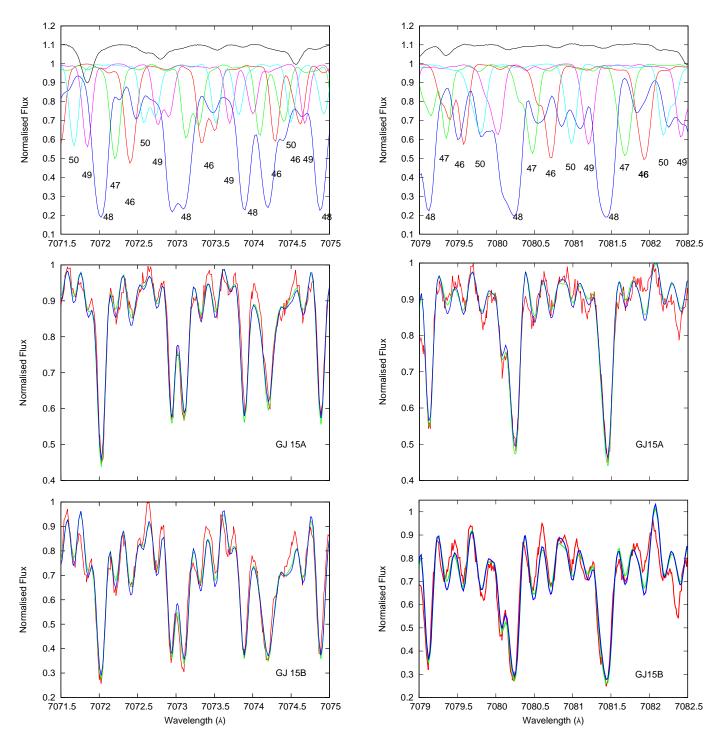
3.2.1. Spectral range x_1

As shown in Sect. 3.1.2, the heads of the (0,1) band of the γ-system of TiO isotopologues form an unresolved blend at 7054 Å, even in HIRES spectra obtained with $R \sim 70\,000$. Some authors used spectral regions beyond 7054 Å to determine the TiO isotope abundance. Spectral ranges $\sim$7071.5–7075 Å and 7079–7082.5 were used by Lambert & Luck (1977) and Clegg et al. (1979) to analyse spectra of M stars. A detailed identification of positions of TiO isotopologues is given in their papers. However, we see from their identifications that nearly all wavelengths receive a contribution from several TiO isotopologues. To illustrate this point, the two upper panels of Fig. 2 show spectra of all TiO isotopologues computed separately. We show here fluxes that were used to create the upper left panel of Fig. 1; at larger scales, these fluxes are shown for the above spectral ranges in the wavelength frame reduced to $V_r = 0$. The strongest features are marked by atomic numbers z of Ti atoms formed by corresponding TiO molecules.

The lower panels of Fig. 2 show fits to spectra of GJ 15A and B for the cases of the solar isotopic ratios of Ti, that is, ^{46}Ti, ^{47}Ti, ^{48}Ti, ^{49}Ti, and ^{50}Ti of 8.3, 7.4, 73.7, 5.4, and 5.2 (De Bievre & Taylor 1993; Lodders et al. 2009), and a modified Ti isotopic ratio, ^{46}Ti, ^{47}Ti, ^{48}Ti, ^{49}Ti, and ^{50}Ti of 10.4, 9.3, 67.0, 6.8, and 6.5, in the latter case, the abundances of ^{48}Ti were reduced by 10%, and the abundances of the other Ti isotopes were increased by 25%. For simplicity we label these modified TiO isotopic abundances as the M25 ratios. The comparison of two spectra illustrates the sensitivity of the selected spectral features to changes of Ti isotopic ratio.

We note that all isotopologue features can be clearly identified in the observed spectra. However, we see only a rather marginal response in these features to the change in Ti isotopic ratios. In all cases we see blends of a few lines of different isotopes, and the dominant contribution of ^{48}TiO. The lines of ^{48}TiO are saturated, which means that they show a rather weak response to isotopic abundance changes. A qualitative by-eye estimate of the comparison of the fine details between the observed and computed spectra seems to suggest a better fit for the case of solar Ti isotope ratios. These fits adopted [Ti] = $A_\odot$(Ti) − A_*(Ti) = −0.1, where $A_\odot$(Ti), A_*(Ti) are abundances of Ti in the atmospheres of the Sun and star, for GJ 15A and −0.2 for GJ 15B.

Fits to the x_1 spectral range for spectra of GJ 15A and GJ 15B using three line lists for TiO isotopologues are presented: S98 from Schwenke (1998), P12 updated from Plez (1998), and TOTO of the Exomol group (McKemmish et al. 2019). Plots with the fits are given in Fig. A.1, which shows fits to the observed spectra in the selected regions, as also illustrated in Fig. 2. We

Fig. 2. *Upper panels*: features created by the TiO isotopologues in the spectral ranges used by Lambert & Luck (1977) and Clegg et al. (1979) to determine the Ti isotopic abundance in M-stars. Theoretical spectra of TiO isotopologues were computed for 3500/5.0/0.0 model atmosphere and solar Ti isotopic ratios. Synthetic spectra are convoluted with $R = 70\,000$. The strongest features are marked by atomic numbers of the Ti isotope in the associated TiO molecule. Black line shows the Arcturus spectrum (Hinkle et al. 1995). *Middle panels*: fits of theoretical spectra computed for 3800/5.0 model atmospheres to the observed spectra of GJ 15A. *Bottom panels*: fits of theoretical spectra computed for 3500/5.0 model atmospheres to the observed spectra of GJ 15B. Observed spectra are denoted by red lines, spectra computed for the solar isotopic abundance are shown by green lines, and spectra computed for M25 isotopic ratios by blue lines.

performed fits to the head of the γ system at 7054 Å. The computed χ^2 minimisation sums are given in Table 3. In all cases, TOTO provides the best fit. We list the conclusions below that we also made from the comparisons.

a) The positions of the strong absorption feature formed by absorption of photons in the ^{48}Ti transitions agree well, but the intensities disagree in some cases.

b) We see more pronounced differences in the positions and intensities for lines belonging to other less abundant TiO isotopologues.

c) The formally computed S parameters that we obtained using different line lists differ from each other, see Table 3.

We note that this rather narrow and phenomenological comparison of the results obtained with different line lists cannot
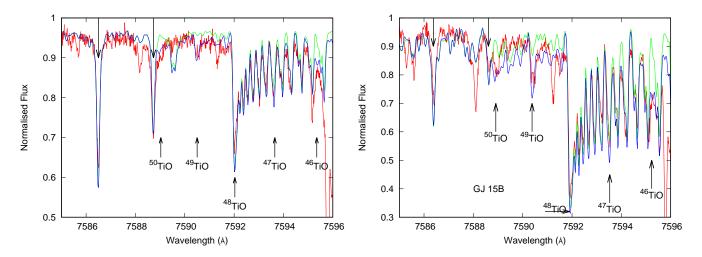
Fig. 3. Fits of our synthetic spectra to the observed GJ 15A (*left panel*) and GJ 15B (*right panel*) spectra with Ti isotopic ratios ^{50}Ti, ^{49}Ti, ^{48}Ti, ^{47}Ti, and ^{46}Ti of 6.2, 7.9, 72.8, 5.2, and 7.9 and 6.0, 5.8, 76.6, 4.2, and 7.4, respectively, shown by blue lines. Observed spectra are shown by red lines, and fluxes computed for ^{48}Ti O alone are shown by green lines. Downward arrows mark Fe I lines.

Table 3. Parameter S computed in the fitting ranges given as wavelengths in Å.

	7053–7060	7071–7084	7580–7594
P12	0.73 ± 0.03 (A)	2.75 ± 0.04	0.75 ± 0.02
	2.11 ± 0.05 (B)	7.60 ± 0.08	3.50 ± 0.04
S98	0.66 ± 0.03 (A)	2.45 ± 0.04	0.76 ± 0.02
	1.64 ± 0.04 (B)	3.64 ± 0.05	3.40 ± 0.04
Толо	0.47 ± 0.02 (A)	1.10 ± 0.03	0.73 ± 0.02
	1.28 ± 0.04 (B)	2.32 ± 0.04	3.19 ± 0.04

Table 4. Isotopologue abundances and Ti abundance in the atmospheres of GJ 15A and GJ 15B.

Isotopologue	The Sun	GJ 15A	GJ 15B
^{46}Ti	8.3	7.9 ± 0.01	7.4 ± 0.3
^{47}Ti	7.4	5.2 ± 0.01	4.2 ± 0.4
^{48}Ti	73.7	72.8 ± 0.01	76.6 ± 0.2
^{49}Ti	5.4	7.9 ± 0.01	5.8 ± 0.3
^{50}Ti	5.2	6.2 ± 0.01	6.0 ± 0.0
[Ti]	0.0	0.040 ± 0.001	0.199 ± 0.003

provide a final conclusion about which is the best list. However, our conclusions are valid for three spectral ranges, which have been used by different authors for Ti isotopic abundance analysis.

However, when we combine our findings with the more sophisticated, deeper, and independent analysis made by McKemmish et al. (2019) and Bernath (2020), we find general agreement that Толо is the best list. Even the by-eye inspection confirms that the Толо line list is better at reproducing the observed features in terms of both line intensities and line positions, see Fig. 3.

3.2.2. Spectral range x_2

The spectral range x_2 is favourably different from x_1. Heads of the TiO bands are well spaced across the wavelengths, which improves their identification and analysis. This is more relevant for the band heads of ^{50}TiO and ^{49}Ti O, which are located before the head of the strong ^{48}TiO band. Despite the strong blending between the ^{50}TiO band head and an Fe I line, the spectral detail is clearly seen in the observed spectrum, which is relevant to stars with low $v \sin i$.

Unfortunately, in the spectra of the two stars, the ^{46}Ti O band head coincides with strong telluric feature. Still, molecular band heads of other TiO isotopologues are seen, therefore we were able to determine all ratios. ^{46}Ti was determined as $100 - (^{47}$Ti $+ ^{48}$Ti $+ ^{49}$Ti $+ ^{50}$Ti). Moreover, we included [Ti] in the minimisation process because the isotopic ratios depend on the abundance of the element, see Fig. 2 in Pavlenko et al. (2020) for the case of

the carbon isotopic ratio determination. Strong and weak features show different responses to abundance variations.

We performed the isotopologue abundance analysis using the determination of min S (^{47}Ti, ^{48}Ti, ^{49}Ti, ^{50}Ti, and [Ti]) for the set of synthetic spectra computed for the grid of input parameters given below:

– ^{47}Ti varies in the range [3.0–10.0] with a step of 1.0;
– ^{48}Ti varies in the range [71.5–77.5] with a step of 0.5;
– ^{49}Ti varies ithe range [3.0–10.0] with a step of 1.0;
– ^{50}Ti varies in the range [3.0–10.0] with a step of 1.0;
– [Ti] varies in the range [0 – 0.1] and [0.1–0.2] with steps of 0.02 for GJ 15A and GJ 15B, respectively.

These parameter ranges were determined in a set of numerical experiments.

Our 5D minimisation procedure provides a set of minimisation sums, S, followed by formally computed errors, ΔS. We obtained $S_{\min} = 1.030 \pm 0.021$ for GJ 15A, and then averaged solutions falling in the window $1.030 < S < 1.052$. For GJ 15B we averaged solutions in the range $3.332 < S < 3.375$. Because the level of noise in the GJ 15B spectrum is higher, our solution is less reliable for this cooler star. Table 4 shows relative abundances of TiO isotopologues determined from the χ^2 fits to the observed spectra of GJ 15A and GJ 15B.

The green lines in Fig. 3 show spectra computed without ^{46}Ti O, ^{47}Ti O, ^{49}Ti O, and ^{50}Ti O. The comparison with the full sample of TiO isotopologues shows the contribution of the less abundant species to the total spectrum.

Generally speaking, in the ideal case of isolated stars of similar masses that form a wide binary system, we do not expect

large differences in their abundances. As a result, any differences in isotopic ratios may be caused by other reasons, which might tell us something about our procedure or about the physical state of the stars. Here, we find good agreement in the fits to the ^{49}Ti O and ^{47}Ti O features, but we also see some disagreement for ^{50}Ti O in the shape and intensity between the computed molecular bands and the observations.

To compare the fits of synthetic spectra in the x_2 spectral using the different line lists S98, P12, and TOTO we computed the parameter. In these computations we adopted solar isotopic ratios for the Ti isotopes. The fits to the observed spectra are shown in Fig. A.2; the computed values of S for all of them are given in Table 3.

We note that the two Fe I lines seen in this spectral range can be fitted with [Fe] = −0.4 for both stars, which confirms the deficit of iron found previously, see Table 1. Our minimisation procedure allows us to determine [Ti] = 0.040 ± 0.001 and 0.199 ± 0.003 for GJ 15A and GJ 15B, respectively.

3.2.3. Spectral ranges x_3−x_5

Unfortunately, TiO is weak in the x_3−x_5 spectral ranges for the observed and computed spectra of GJ 15A and GJ 15B. The x_3 spectral range is dominated by an Na I line; here we see only a weak ^{48}TiO band head. This spectral range may be more useful for giant spectra, where the Na I 8200 Å subordinate triplet is much weaker. The isotopologue bands are here in ascending order, that is, from ^{46}Ti O to ^{50}TiO, which is the opposite order to the x_2 spectral range.

As we noted above, the molecular bands of the TiO isotopologues in the x_4 spectral range form a single feature in the observed and computed spectra, as in x_1 spectral range. We cannot distinguish contributions from TiO isotopologues in the spectra of GJ 15A and GJ 15B because TiO appears much weaker here and there is strong pollution by telluric lines.

In the x_5 spectral range we observe a descending order of the isotopologue bands, similar to x_2. However, the TiO absorption is too weak here to form any notable features that might be used in the analysis.

4. Discussion

Although molecular spectroscopy of TiO provides the most accurate method of determining the titanium isotope abundance in cool stars, the analysis of TiO spectroscopy is very challenging. As a heavy molecular system, the TiO spectra is complex, with spectral features that formed by blends of many absorption lines, often from different isotopologues. To obtain high-accuracy measurements, it is vital to select the best spectral region for the high-resolution analysis.

The main aims of this paper are (a) to test the new TOTO TiO line list to determine the TiO isotopologue abundances in the observed spectra of cool M dwarfs, (b) to determine the most appropriate spectral ranges in which the Ti isotope abundances in their atmospheres can be determine, and (c) to retrieve the Ti isotopic ratios for GJ 15A and GJ 15B to test the performance of this method.

4.1. Line list accuracy

Previous comparisons of TiO line lists (e.g. by McKemmish et al. 2019; Bernath 2020; Piette et al. 2020) have concluded that the TOTO line list is generally superior to previously assembled line lists. However, these comparisons did not explicitly

consider the quality of the predicted isotopologue spectra, that is, how accurately each line list reproduces the astronomically observed isotopologue frequency shifts and therefore allows the abundance of different titanium isotopes to be accurately measured astronomically. We here modelled several spectral regions that can be used for a Ti isotope abundance analysis in cool stars, and we compared our model isotopologue spectra that were computed using the TOTO line list with other available line lists. The detailed comparisons with high-resolution M-dwarf spectra with different line lists showed that the TOTO line list performs much better than the earlier line lists, particularly in matching line positions, see Fig. A.1.

4.2. Best spectral ranges for isotope determination

In the past, most researchers have concentrated on analysing the fine details of absorption spectra formed in the redward degrading (0,0) band of the TiO γ band system. However, observable features here are formed by blends of many lines belonging to different isotopologues. In our case, synthetic spectra computed for the solar Ti isotopic ratios in our x_1 spectral range can be fitted to the observed spectra of GJ 15A and GJ 15B; but we found here a rather weak dependence on the reasonable changes (25%) of the TiO isotopologue abundances.

We investigated a few possible spectral ranges and found that the x_2 spectral range is the most useful because the region contains band heads for four of the five stable TiO isotopologues, which suffices to determine all titanium isotope abundances. The ^{46}Ti O band head is severely blended by telluric feature, but ^{46}Ti can be determined as ^{46}Ti = 100−(^{47}Ti + ^{48}Ti + ^{49}Ti + ^{50}Ti).

Our analysis of band heads in the x_2 spectral range provides more reliable abundances of TiO isotopologues, especially of ^{50}TiO and ^{49}TiO, which are not blended by strong lines of ^{48}TiO. Conversely, this spectral range is very interesting because some nucleosynthesis computations predict a large deviation of the ^{50}Ti and ^{49}Ti from the solar abundances at the early epochs of the evolution of our Universe, see the Introduction.

We developed a new procedure that allowed us to determine all Ti isotope abundances together with the Ti abundance using this spectral region. To determine the best solution, we applied a 5D minimisation procedure with input parameters ^{47}Ti, ^{48}Ti, ^{49}Ti, ^{50}Ti, and the titanium abundance [Ti] to take the dependence of the determined isotopic ratios on the adopted titanium abundance into account. In this way, we determined the titanium isotopic ratios and abundance of Ti from our analysis of x_2 spectral range in the framework of the self-consistent approach. This a the key part of our procedure that we developed to analyse TiO isotopologue abundances. Furthermore, to obtain statistically significant results, we implemented a special procedure as part of our solution determination: the sets of the best solutions were sorted in the ascending order of the minimisation sums S, and the corresponding isotopic ratios and Ti abundances were averaged across $S_{\min} - \Delta S \leq S \leq S_{\min}$, where $S_{\min}$ and ΔS are the minimum S and the formal error of its determination S, see Sect. 2.4.

4.3. Analysis of GJ 15A and GJ 15B spectra

In our study, we modelled TiO spectra of two stars that form a binary system, specifically, the CARMENES spectra of two M dwarfs, GJ 15A and GJ 15B, in the spectral ranges of our interest. We selected GJ 15A and GJ 15B because (a) they are comparatively well studied and (b) they are slow rotators. We anticipated that the isotope abundance in both stars should be

equal and thus we could use the binarity of the system to prove the reliability of our results when (a) we know all abundances in the atmospheres of both stars, (b) their effective temperatures are well determined from the fits to observed spectral energy distributions; (c) model atmospheres are computed for the found $T_{\rm eff}$, log g and abundances, and d) spectra of both components were observed with the same high quality. Unfortunately, none of these conditions were entirely satisfied. We fixed $T_{\rm eff} = 3800$ K for GJ 15A, and $T_{\rm eff} = 3500$ K for GJ 15B, and adopted log g = 5.0 for both stars because the system is rather old, see Table 1. Furthermore, GJ 15B is fainter, and the S/N of the obtained spectrum for the cooler dwarfs is lower than that of GJ 15A.

Our best fits to the observed spectra of GJ 15A and GJ 15B in the x_2 spectral range provide non-solar Ti isotopic ratios of ^{46}Ti, ^{47}Ti, ^{48}Ti, ^{49}Ti, and ^{50}Ti of 7.9, 5.2, 72.8, 7.9, and 6.2 for GJ 15A (M1 V) and 7.4, 4.2, 76.6, 5.8, and 6.0 for GJ 15B (M3 V) with an accuracy of ±0.2. Furthemore, [Ti] = 0.040 and 0.199 with an accuracy ±0.10 was also determined for GJ 15A and GJ 15B, respectively. The differences in the isotope abundances between the two stars are significantly larger than the uncertainties of each individual determination. It is unclear whether these differences reflect actual differences in the isotope abundances in the two stellar objects, inaccuracies in the determination of the relevant physical properties of both systems (e.g. temperature), or can be attributed to modelling uncertainties. For more definite conclusions, an abundance analysis for all elements should be considered in both stars. Ideally, the observed spectra of both M dwarfs should be of the same quality, that is, have the same resolution and S/N.

We note some disagreement in the shape and intensity between the computed molecular bands of ^{50}Ti O and the observations. Likely, here we have some contribution of other unidentified molecule(s). Given the promise of this spectral region in determining titanium isotope abundances, we suggest detailed consideration of this issue in the future.

We anticipated that pecularities in abundances can be explained by the inaccuracies of $T_{\rm eff}$ determination, for instance, we found that lowering $T_{\rm eff}$ of GJ 15A by 100 K reduces the Ti abundance for the star by −0.15. Furthermore, the Ti I line seen in the lower panels of Fig. A.3 can be fitted by adopting [Ti] = −0.2. However, this Ti abundance describes the Ti line in GJ 15A better. To describe the Ti line in the GJ 15B spectrum, we should adopt a larger titanium abundance. Furthermore, from the fit to the x_2 spectral range, we obtained larger [Ti] in the atmosphere of GJ 15B.

Of note, we found that the binary seems to be Fe deficient, as previously reported by several authors, see Table 1. To obtain reasonable fits to the two Fe I lines observed in the x_2 spectral range, we adopted [Fe] = −0.4, see Fig. 3. Conversely, we obtained a rather solar abundance of Ti in the atmospheres of two stars. Temperature changes cannot explain the observed overabundance of Ti with respect to Fe. The overabundance of Ti with respect to Fe can be interpreted, at least qualitatively, as due to an α-element abundance enhancement in metal-poor stars, see the Introduction.

5. Conclusions

An accurate determination of titanium isotope abundances can shed new light on astrophysical processes. On the large scale, comparing isotope abundances in atmospheres of the slowly evolving M dwarfs to abundances in more massive, fast evolving M giants could provide new information about the evolutionary processes in our Galaxy. In individual astrophysical systems,

such as the Earth-Moon system and host star-exoplanet systems, more local histories can be determined, for example, near-identical titanium (and oxygen) isotope abundances on Earth and the Moon challenge the dominant theory that the Moon formed after a giant impact, see the Introduction.

Our results demonstrate that titanium isotope abundances in M stars can be most effectively measured using high-resolution spectroscopy of TiO in the x_2 spectral region, that is, air wavelengths of 7580–7594 Å, through fitting observed spectral intensities of many isotopologue features against models computed using the ToTo line list. The successes and limitations of this method were explored through detailed studies of the spectroscopy of the GJ 15A and GJ 15B binary system. We find that for optimal results, $T_{\rm eff}$, log g, and the abundances of all elements should be determined by the most accurate procedure and the spectra of all M dwarfs should be of the same very high quality. Taking into account all uncertainties of our analysis, we conclude that our determinations are accurate to ~5% of the absolute abundance of the main isotopologue and to 20–30% of the relative abundances of minor isotopologues. The use of better quality spectra will increase these accuracies by a factor of 10. Fortunately, the spectral range of our interest, that is, x_2, lies in the NIR, where observed fluxes are higherer than in optical wavelengths, and detectors provide data of higher S/N.

References

Alexander, C. M. O., & Nittler, L. R. 1999, ApJ, 519, 222
Allard, F. 2014, IAU Symp., 299, 271
Allard, F., Hauschildt, P. H., & Schwenke, D. 2000, ApJ, 540, 1005
Anders, E., & Grevesse, N. 1989, Geochim. Cosmochim. Acta, 53, 197
Bernath, P. 2020, ApJ, 895, 87
Cenarro, A. J., Peletier, R. F., Sánchez-Blázquez, P., et al. 2007, MNRAS, 374, 664
Chavez, J., & Lambert, D. L. 2009, ApJ, 699, 1906
Ciddor, P. E. 1996, Appl. Opt., 35, 1566
Clegg, R. E. S., Lambert, D. L., & Bell, R. A. 1979, ApJ, 234, 188
De Bievre, P., & Taylor, P. 1993, Int. J. Mass Spectr. Zon Process., 123, 149
Furtenbacher, T., Császár, A. G., & Tennyson, J. 2007, J. Mol. Spectr., 245, 115
Gaia Collaboration (Brown, A. G. A., et al.) 2018, A&A, 616, A1
Gaidos, E., & Mann, A. W. 2014, ApJ, 791, 54
Gaidos, E., Mann, A. W., Lépine, S., et al. 2014, MNRAS, 443, 2561
Gautier, T. N., I., Rieke, G. H., Stansberry, J., et al. 2007, ApJ, 667, 527
Hinkle, K., Wallace, L., & Livingston, W. 1995, PASP, 107, 1042
Hoeijmakers, H. J., de Kok, R. J., Snellen, I. A. G., et al. 2015, A&A, 575, A20
Howard, A., Marcy, G., Fischer, D., et al. 2014, ApJ, 794, 1
Hughes, G. L., Gibson, B. K., Carigi, L., et al. 2008, MNRAS, 390, 1710
Kobayashi, S., Nishimiya, N., & Suzuki, M. 2019, Spectrochim. Acta Part B At. Spectr., 152, 30

Koleva, M., & Vazdekis, A. 2012, A&A, 538, A143
Kurucz, R. L. 2011, Can. J. Phys., 89, 417
Lambert, D. L., & Luck, R. E. 1977, ApJ, 211, 443
Lambert, D. L., Mallia, E. A., & Smith, G. 1972, Sol. Phys., 26, 250
Lippincott, S. L. 1972, AJ, 77, 165
Lodders, K., Palme, H., & Gail, H. P. 2009, Landolt Börnstein, 4B, 712
Mann, A. W., Feiden, G. A., Gaidos, E., Boyajian, T., & von Braun, K. 2015, ApJ, 804, 64
McKemmish, L. K., Masseron, T., Sheppard, S., et al. 2017, ApJS, 228, 15
McKemmish, L. K., Masseron, T., Hoeijmakers, J., et al. 2019, MNRAS, 488, 2836
Mochizuki, Y., & Kumagai, S. 2004, AIP Conf. Proc., 704, 369
Mochizuki, Y., Takahashi, K., Janka, H. T., Hillebrand t, W., & Diehl, R. 1999, A&A, 346, 831
Newton, E. R., Charbonneau, D., Irwin, J., et al. 2014, AJ, 147, 20
Passegger, V. M., Reiners, A., Jeffers, S. V., et al. 2018, A&A, 615, A6
Pavlenko, Y. V. 1997, Astron. Rep., 41, 537
Pavlenko, Y. V. 2014, Astron. Rep., 58, 825
Pavlenko, Y. V., Rebolo, R., Martin, E. L., & Garcia Lopez, R. J. 1995, A&A, 303, 807
Pavlenko, Y., Suárez Mascareño, A., Rebolo, R., et al. 2017, A&A, 606, A49
Pavlenko, Y. V., Yurchenko, S. N., & Tennyson, J. 2020, A&A, 633, A52
Piette, A. A., Madhusudhan, N., McKemmish, L. K., et al. 2020, MNRAS, 496, 3870
Plez, B. 1998, A&A, 337, 495
Polyansky, O. L., Kyuberis, A. A., Lodi, L., et al. 2017, MNRAS, 466, 1363
Prugniel, P., Vauglin, I., & Koleva, M. 2011, A&A, 531, A165
Reid, I. N., Hawley, S. L., & Gizis, J. E. 1995, AJ, 110, 1838

Reiners, A., Zechmeister, M., Caballero, J. A., et al. 2018, A&A, 612, A49
Rudolf, N., Günther, H. M., Schneider, P. C., & Schmitt, J. H. M. M. 2016, A&A, 585, A113
Ryabchikova, T., & Pakhomov, Y. 2015, Balt. Astron., 24, 453
Schlieder, J. E., Lépine, S., Rice, E., et al. 2012, AJ, 143, 114
Schwenke, D. W. 1998, Faraday Discuss., 109, 321
Taylor, G. J. 2012, Titanium Isotopes Provide Clues to Lunar Origin, Planetary Science Research Discoveries Report
Tennyson, J. 2019, Astronomical Spectroscopy : An Introduction to the Atomic and Molecular Physics of Astronomical Spectra, 3rd edn. (Singapore: World Scientific)
Tennyson, J., & Yurchenko, S. N. 2012, MNRAS, 425, 21
Tennyson, J., Yurchenko, S. N., Al-Refaie, A. F., et al. 2016a, J. Mol. Spectr., 327, 73
Tennyson, J., Lodi, L., McKemmish, L. K., & Yurchenko, S. N. 2016b, J. Phys. B: At. Mol. Opt. Phys., 49, 102001
Terrien, R. C., Mahadevan, S., Deshpande, R., & Bender, C. F. 2015, ApJS, 220, 16
Timmes, F. X., Woosley, S. E., & Weaver, T. A. 1995, ApJS, 98, 617
Tóbiás, R., Furtenbacher, T., Tennyson, J., & Császár, A. G. 2018, Phys. Chem. Chem. Phys., 21, 3473
Valenti, J. A., Piskunov, N., & Johns-Krull, C. M. 1998, ApJ, 498, 851
van Buren, D., Brundage, M., Ressler, M., & Terebey, S. 1998, AJ, 116, 1992
Woosley, S. E., & Weaver, T. A. 1994, ApJ, 423, 371
Wyckoff, S., & Wehinger, P. 1972, ApJ, 178, 481
Yurchenko, S. N., Lodi, L., Tennyson, J., & Stolyarov, A. V. 2016, Comput. Phys. Commun., 202, 262
Zboril, M., & Byrne, P. B. 1998, MNRAS, 299, 753
Zhang, J., Dauphas, N., Davis, A., Leya, I., & Fedkin, A. 2012, Nat. Geosci., 5, 251

Appendix A: Some additional stuff

Table A.1. Example of input data of ^{47}Ti O lines in our computation.

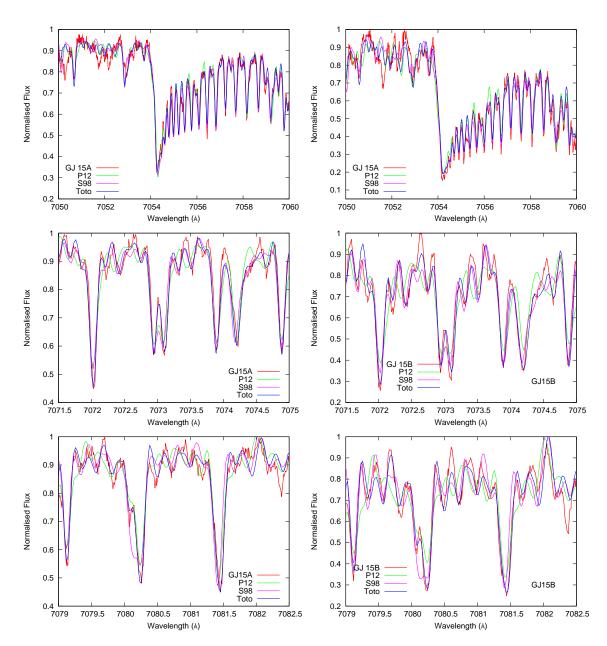| λ (A) in air	gf	E'' (eV)
3493.707	3.172E-05	0.890
3493.707	3.172E-05	0.890
3494.907	3.323E-05	0.897
3494.907	3.323E-05	0.897
3496.134	3.481E-05	0.903
3496.134	3.481E-05	0.903
3496.479	3.521E-05	0.917
3496.479	3.521E-05	0.917
3497.389	3.647E-05	0.910
3497.389	3.647E-05	0.910
...		

Fig. A.1. Comparison of fits to the observed TiO features in the x_1 spectral range in GJ 15A (*left panels*) and GJ 15B (*right panels*) using line lists of different authors. Here solar isotopic ratios of Ti were adopted.
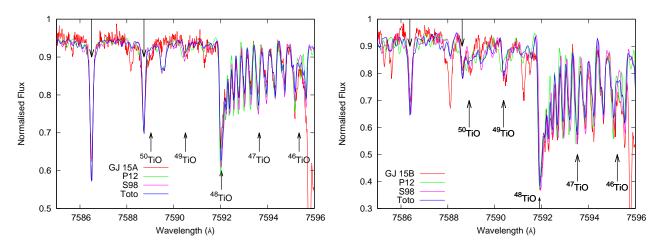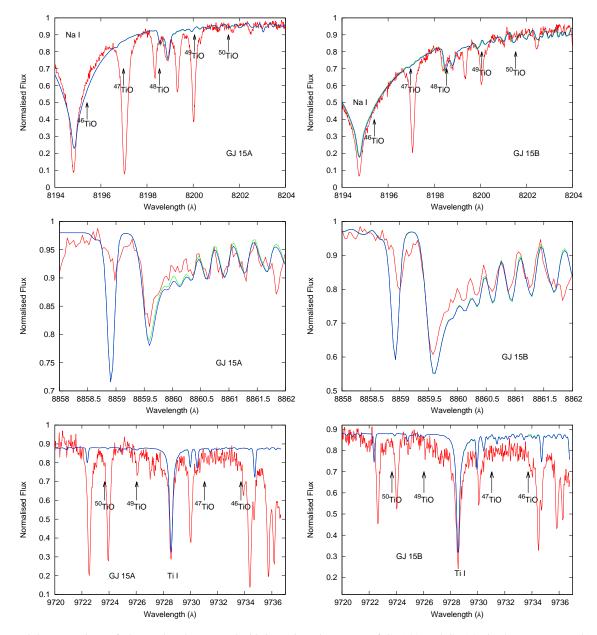
Fig. A.2. Comparison of fits to the observed TiO features in the x_2 spectral range in GJ 15A (*left panel*) and GJ 15B (*right panel*) using line lists of different authors. Here solar isotopic ratios of Ti were adopted.

Fig. A.3. *Top left*: comparison of observed and computed TiO isotopic ratio spectra of GJ 15A and GJ 15B in the x_3 (*top panels*), x_4 (*middle panels*), and x_5 (*bottom panels*) spectral ranges for solar (green line) and M25 (blue line) abundance ratios.